Nano Research 2018, 11(3): 1554–1562
https://doi.org/10.1007/s12274-017-1771-4
Research Article

ISSN 1998-0124
CN 11-5974/O4

Dip-coating processed sponge-based electrodes for stretchable Zn-MnO_2 batteries

Hong-Wu Zhu[§], Jin Ge[§], Yu-Can Peng, Hao-Yu Zhao, Lu-An Shi, and Shu-Hong Yu (✉)

Division of Nanomaterials & Chemistry, Hefei National Laboratory for Physical Sciences at the Microscale, Collaborative Innovation Center of Suzhou Nano Science and Technology, Department of Chemistry, CAS Centre for Excellence in Nanoscience, Hefei Science Centre of CAS, University of Science and Technology of China, Hefei 230026, China

[§] *Hong-Wu Zhu and Jin Ge contributed equally to this work.*

Received: 22 May 2017
Revised: 16 July 2017
Accepted: 18 July 2017

KEYWORDS
stretchable battery,
Zn-MnO_2 battery,
silver nanowires,
sponge,
binary network structure

ABSTRACT

Stretchable electronics are in high demand for next-generation wearable devices, but their fabrication is still challenging. Stretchable conductors, flexible pressure sensors, and foldable light-emitting diodes (LEDs) have been reported; however, the fabrication of stable stretchable batteries, as power suppliers for wearable devices, is significantly behind the development of other stretchable electronics. Several stretchable lithium-ion batteries and primary batteries have been fabricated, but their low capacities and complicated manufacturing processes are obstacles for practical applications. Herein, we report a stretchable zinc/manganese-oxide (Zn-MnO_2) full battery based on a silver-nanowire-coated sponge prepared via a facile dip-coating process. The spongy electrode, with a three-dimensional (3D) binary network structure, provided not only high conductivity and stretchability, but also enabled a high mass loading of electrochemically active materials (Zn and MnO_2 particles). The fabricated Zn-MnO_2 battery exhibited an areal capacity as high as 3.6 mAh·cm^{-2} and could accommodate tensile strains of up to 100% while retaining 89% of its original capacity. The facile solution-based strategy of dip-coating active materials onto a cheap sponge-based stretchable current collector opens up a new avenue for fabricating stretchable batteries.

1 Introduction

Stretchable electronics, which can sustain large deformations and intimately integrate with curvilinear surfaces, have drawn significant attention due to the high demand for next-generation wearable and implantable devices [1–4]. With the development of stretchable conductors, various stretchable devices, such as health-monitoring patches [5], smart clothes [3, 6], and electronic skin [4], have been demonstrated. However, developing stable power supplies with adaptable stretchability for wearable devices is

Address correspondence to shyu@ustc.edu.cn

challenging [7]. The primary challenge in fabricating stretchable batteries lies in preparing a stable, stretchable, and highly porous current collector, which can not only maintain stable electrical conductivity under deformation, but also possess a large surface area for loading a sufficient amount of electrochemically active materials.

Traditional batteries are built using rigid metal-foil current collectors, which suffer structural failure under deformation [8]. Two promising strategies have been proposed for replacing these metal foils: geometric structuring of traditional metal electrodes and preparation of intrinsically stretchable porous electrodes [9]. In terms of geometric structuring, several delicate structures, such as wavy structures [10], zigzag stripes [11], serpentine interconnects [12, 13], origami [14], and helical springs [15], have been demonstrated. Using a spatial structural design endows the rigid conductive materials with a certain degree of buffer that prevents the materials themselves directly bearing a deformation. However, such electrode materials might crack and drop off under strain, due to their low surface area and varying conductivity [16]. The intrinsic stretchability and relatively high surface area of stretchable porous electrodes render them more suitable for fabricating stretchable batteries [17]. Conductive nanomaterials such as carbon nanotubes (CNTs) [18], carbon films [19], metal nanowires (NWs) [20], and metal nanoparticles [21] have been widely used for fabricating stretchable electronics and have shown potential as three-dimensional (3D) stretchable electrodes. Among these materials, CNTs are the most commonly used for fabricating stretchable current collectors owing to their high mechanical strength and chemical stability [22]. For example, CNTs have been spun into micro-fibers to fabricate various fibrous energy devices, such as solar cells [1], supercapacitors [23], and lithium-ion batteries [24]. However, considering the superior conductivity of metallic conductors, CNTs might not provide optimal battery performance [25]. The conductivity of CNTs could be enhanced by using micrometer-sized silver flakes as a conductive filler [26].

3D porous metal frameworks have been used as rigid current collectors [27]. Assembling metallic materials on porous elastomers has provided some success for obtaining stretchable and conductive metallic frameworks. Various metals have been directly deposited onto fabrics to prepare stretchable conductors using electron beam evaporation [13], thermal evaporation [28], and electrodeposition [29]. In particular, silver nanowires (AgNWs) have been used as conductive building blocks to fabricate stretchable electronics [20, 30]. A binary-network structure design, consisting of 2D networks of AgNWs percolated into a 3D skeleton of commercial polyurethane sponge (PUS), exhibited excellent conductivity and stretchability [30].

Herein, we demonstrate a facile all-solution process for preparing a stretchable zinc/manganese-oxide (Zn-MnO_2) primary battery using a porous 3D AgNW binary network (PUS@AgNW) as a stretchable current collector. AgNWs were dip coated onto a PUS skeleton to form the binary-network structure, which was used as a stretchable porous current collector. By tracking the transformation process during deformation, we found that the structure effectively dispersed the deformation, with the individual PUS microfibers enduring a deformation less than that of the overall PUS@AgNW structure. Electrochemically active materials (Zn and MnO_2) were dip coated onto the PUS@AgNW current collector to complete the electrode construction [31]. The porous structure of PUS@AgNW enabled high mass loading and intimate contact between the current collector and the electrochemically active particles, which occupied open pores. The prepared stretchable Zn-MnO_2 full battery exhibited a capacity of up to 3.6 $mAh \cdot cm^{-2}$ with a 12 $mg \cdot cm^{-2}$ MnO_2 loading. Several such batteries connected in series could power a circuit loaded with an LED under repeated strain. Under 100% strain, the battery still maintained 89% capacity, and provided stable power at currents of 0.35, 0.7, and 1 mA. Compared with previously reported complicated nanofabrication processes, the entire battery preparation process reported here is simple and can be easily scaled up, with the resultant stretchable battery satisfying the energy-supply requirements for stretchable electronics [13].

2 Experimental

2.1 Preparation of the electrodes

A detailed description of the preparation process is

provided in the Electronic Supplementary Material (ESM). Briefly, commercially available PUS was washed using deionized water (DIW) and ethanol separately, and then dried and cut into small slices. The cleaned sponge slices were thoroughly immersed in a 1 wt.% polydimethyldiallylammonium chloride (PDDA) (M_W = 100,000–200,000) solution overnight. PUS@AgNW current collectors were prepared by dropping a 7.5 mg·mL^{-1} AgNW ethanol solution onto the modified PUS slices. The slices were then heated in an oven at 80 ℃ for 30 min to evaporate the excess ethanol. Afterwards, the PUS@AgNW current collectors were baked at 180 ℃ for 20 min to weld the AgNWs to the PUS. Electrodes were prepared by dropping "Zn ink" and "MnO_2 ink" onto PUS@AgNW current collectors using a Pasteur pipette. Finally, the electrodes were dried at 120 ℃ for 30 min to remove residual water.

2.2 Cell assembly

A piece of acrylic elastomer (3M VHB 4910) was cut into a well to house the electrodes and the electrolyte. The well was then put onto a piece of elastomer to form a little chamber. A cathode and an anode were put on the top of the chamber side by side with a ~ 5 mm gap, leaving the PUS@AgNW parts to connect to the external circuit. After filling the porous electrode and the chamber with a prepared electrolyte gel, another piece of elastomer was put on the top of the cell to seal it.

2.3 Measurements and characterization

Electrochemical characterization was performed using galvanostatic discharge and electrochemical impedance spectroscopy (EIS) measurements using a CHI 760D electrochemical workstation (CH instruments). The EIS measurements were conducted using a 10 mV fluctuating potential from 100,000 Hz to 10 Hz at an open circuit voltage (OCV) (1.5 V). The microstructure of the sponge was investigated using scanning electron microscope (SEM) (Zeiss Supra 40, 5 kV). Powder X-ray diffraction (PXRD) was carried out using an X-ray diffractometer (TTRIII, Rigaku, Japan) with Cu Kα radiation (λ = 1.54178 Å). Optical microstructure images of the PUS at different tensile strains were obtained using a microscope (IX71, OLYMPUS, Japan).

3 Results and discussion

High-quality AgNWs with a length of 4–15 μm were synthesized using a previously reported one-pot synthesis method (more details in the ESM) [30]. Commercial PUS was first cleaned and modified with PDDA to endow it with a positively charged surface and facilitate adsorption of the weakly negatively

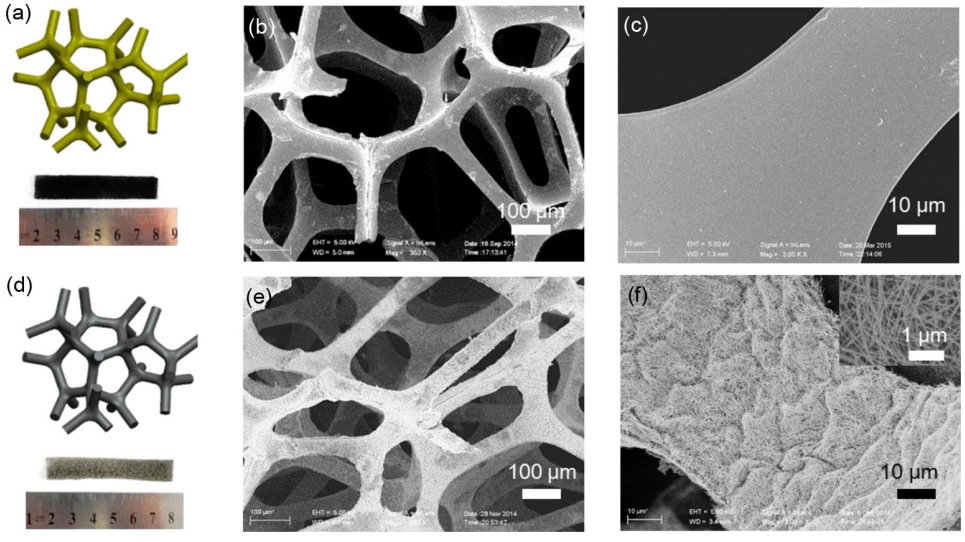

Figure 1 Fabrication process and microstructure of PUS@AgNW material. (a) Schematic of sponge microstructure, and (b) change in the color of the bare PU sponge slice from black to brown after a dip-coating process to prepare the conductive PUS@AgNW material. (b) and (c) SEM images of the bare sponge with a three-dimensional network structure. (e) and (f) SEM images of PUS@AgNW at different magnifications and the surface AgNW networks on the surface of the PU fibers.

charged AgNWs via the electrostatic force. As shown in Fig. S1(a) (in the ESM), the modified PUS was impregnated with a 7.5 mg·mL^{-1} AgNW ethanol solution. After evaporation of the ethanol, the black PUS (Fig. 1(a)) became yellow brown (Fig. 1(d)). The electrode was then annealed (heat welded) at 180 ˚C for 20 min. The conductivity of the PUS@AgNW material could feasibly be tuned by varying the dip-coating times and AgNW concentration, which would change the mass loading of AgNWs on the PUS micro-fiber network.

The microstructure of the sponge skeleton after the dip-coating process was characterized using SEM. The bare PUS had a 3D hierarchical structure, with a pore size of about 400 μm and a fiber diameter of 50 μm (Figs. 1(b) and 1(c)). High-magnification SEM images of PUS@AgNW revealed that the AgNWs were uniformly distributed throughout the sponge network in a wave-like film manner (Figs. 1(e) and 1(f)), which arose from shrinkage of the sponge during the swelling-drying process (Fig. S1(a) in the ESM). This wavy structure was similar to the previously reported structure constructed on the PDMS surface, and maintained connectivity between the AgNWs during stretching [10].

The heat-welding process was used to improve the conductivity and mechanical properties of PUS@AgNW [32]. Prior to heat welding, the AgNWs were in loose contact with one other due to the presence of a 1 to 3 nm thick layer of PVP surfactant. After heat wielding, the total resistance of the PUS@AgNW materials (6 cm × 1 cm × 0.2 cm) typically decreased from several ohms to 1–2 ohms. SEM characterization (Fig. S1(b) in the ESM) showed that the AgNWs melted into nodes after heating at 180 ˚C, while, the XRD pattern in Fig. S1(c) in the ESM indicates that no Ag_2O was generated during this process. Using a welding temperature above 180 ˚C would have resulted in oxidation of the AgNWs and the formation of Ag_2O nanoparticles, leading to a sharp decrease in conductivity.

Optical microscopy was used to track the transition of PUS@AgNW from 0 to 100% strain (Figs. 2(a)–2(e)).

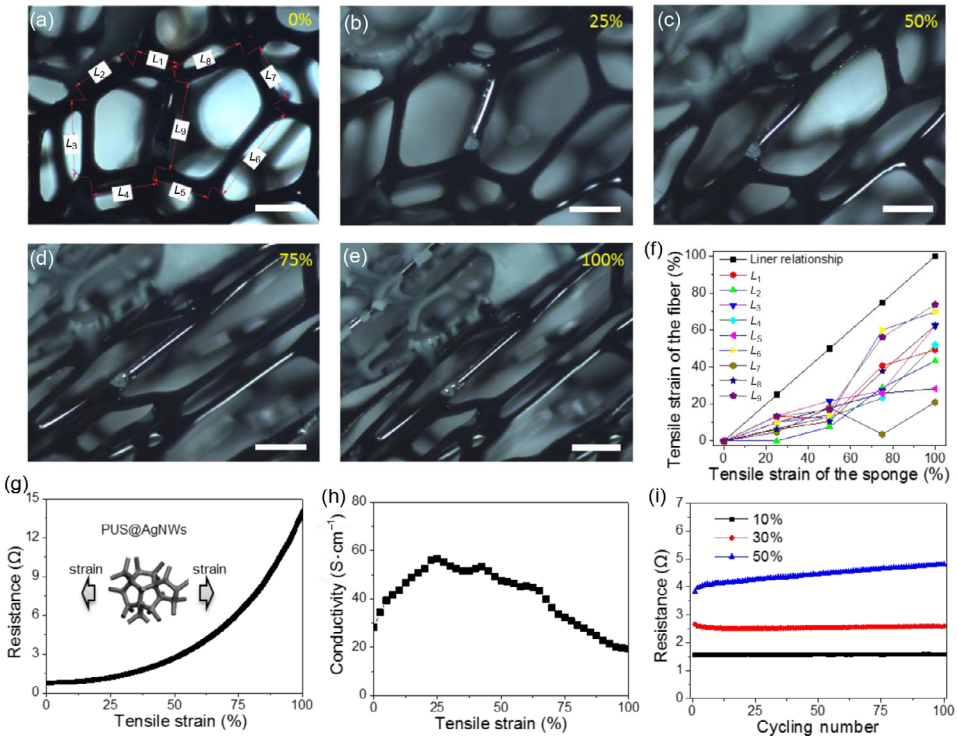

Figure 2 Observation of stretching process and mechanical-electric properties of stretchable PUS@AgNW materials. (a)–(e) Shape transition at the same position on a piece of PUS (a white dot marks the position) under 0, 25%, 50%, 75%, and 100% strain (scale bars: 200 μm). (f) Variation of the length of several PUS fibers marked L_1–L_9 as a function of the tensile strain (up to 100% in the first stretch). Resistance (g) and conductivity (h) of PUS@AgNW as a function of tensile strain (up to 100% in the first stretch). (i) Curves of resistance peak points for each cycle of PUS@AgNW deformation under 0–30% strain and 0–50% strain as a function of the cycle number.

As the strain increased, the PUS micropores tended to shrink perpendicular to the tensile direction. This shape deformation of the PUS skeleton at the micro-scale would mitigate the accumulation of uniaxial strain on the individual struts [33]. Nine PU microfibers, marked L_1–L_9, were selected as representative of the entire porous structure. As shown in Fig. 2(f), the fibers elongated on introducing strain. The strain of a single fiber was always lower than the strain of the whole sponge from 0 to 100%. The length of L_1, L_3, L_8, and L_9, which were aligned in the elongation direction, increased a little more than the average increase. However, the perpendicular fiber (L_7) shrank on increasing the strain from 50% to 100%.

The strain-resistance variation of PUS@AgNW with a 9 mg loading of AgNWs was further investigated. As shown in Fig. 2(h), the resistance of a 6 cm long piece of PUS@AgNW was initially ~ 1 Ω (conductivity: 28 S·cm^{-1}), and slowly increased to 3 Ω, maintaining high conductivity (conductivity: 50 S·cm^{-1}, Fig. 2(h)) under 50% strain. When the sample was stretched from 50% to 100%, the resistance increased from 3 to 14 Ω (conductivity: 20 S·cm^{-1}) due to disconnection of the AgNWs. Interestingly, the conductivity of PUS@AgNW peaked (50 S·cm^{-1}) around 50% strain (Fig. 2(h)), indicating that the silver network is optimized at this level of strain. The PUS@AgNW material had a foam structure with a negative Poisson ratio (NPR) [34]. Figure S1(d) in the ESM shows the change in the width and length of the entire sponge sample (6 cm × 1 cm × 0.2 cm) under strain. From 0 to 50% strain, obvious shrinkage occurred through pore deformation. At around 50% strain, the slope of the curve began to decrease. When the strain exceeded a certain extent (~ 50%), the microfibers directly endured the strain, and displacement of the AgNWs on the nanoscale occurred, resulting in a significantly decrease conductivity on increasing the strain from 50%–100%.

A control sample consisting of a flat AgNW film on a 3M acrylic elastomer was fabricated and tested under stretch deformation. The resistance of the AgNW film increased sharply from 1 to 20 Ω at a strain of 50% (Fig. S2(b) in the ESM), while the resistance of PUS@AgNW was only 3 Ω at the same strain level (Fig. 2(g)). After the first stretch at 50% strain, many unrecoverable cracks appeared on the AgNW film (Fig. S2(c) in the ESM), while the AgNW networks on the PUS surface were maintained, with only small cracks on the joints (marked as red in Fig. S2(d) in the ESM). To demonstrate its robustness, PUS@AgNW was repeatedly stretched to 10%, 30%, and 50% strain 100 times (Fig. 2(i)). The peak point of resistant in each cycle reached a stable level after the first stretch. This was due to the superior 3D-binary-network configuration of PUS@AgNW, which significantly limited disconnection of the AgNWs during deformation.

Electrode materials were easily loaded onto the PUS@AgNW current collector via impregnation using prepared electrochemical inks. The electrochemical inks were prepared by first mixing sufficient amounts of electrochemically active particles (Zn or MnO_2), a conductive additive (carbon black), an aqueous polyoxyethylene (PEO), and DIW using a pestle and mortar [35]. After drying, a uniform particle distribution was observed in both the anode and cathode (Figs. 3(b) and 3(d)). Energy dispersive spectroscopy (EDS) mapping of Zn and Mn (Figs. S3(a) and S3(b) in the ESM) also indicated that electrode materials were homogeneously distributed. High-resolution SEM images (Figs. 3(c) and 3(e)) showed that the Zn and MnO_2 particles were tightly decorated on the surface of the AgNW network, which would facilitate electron transfer from the current collector to the active materials. 3M acrylic was used as a sealing material to package the battery, due to its softness and excellent stretchability (Fig. S2(a) in the ESM). The assembled Zn-MnO_2 stretchable cell was filled with a polyacrylic-acid (PAA)-based polymer gel electrolyte (PGE) and exhibited an OCV of 1.5 V.

No silver oxide phase was observed in the XRD patterns (Figs. 3(f) and 3(g)) of both electrodes, indicating that the AgNWs were stable during the battery fabrication process. Besides the peaks assigned to Ag, the residual peaks matched well with the standard XRD patterns of MnO_2, graphite, Zn, ZnO, and Bi_2O_3. The battery was assembled with the anode and cathode arranged in parallel to form a circuit, which was effective for avoiding electrode shorting [36]. One way to increase the voltage provided by a battery to a sufficient level is to connect multiple batteries in

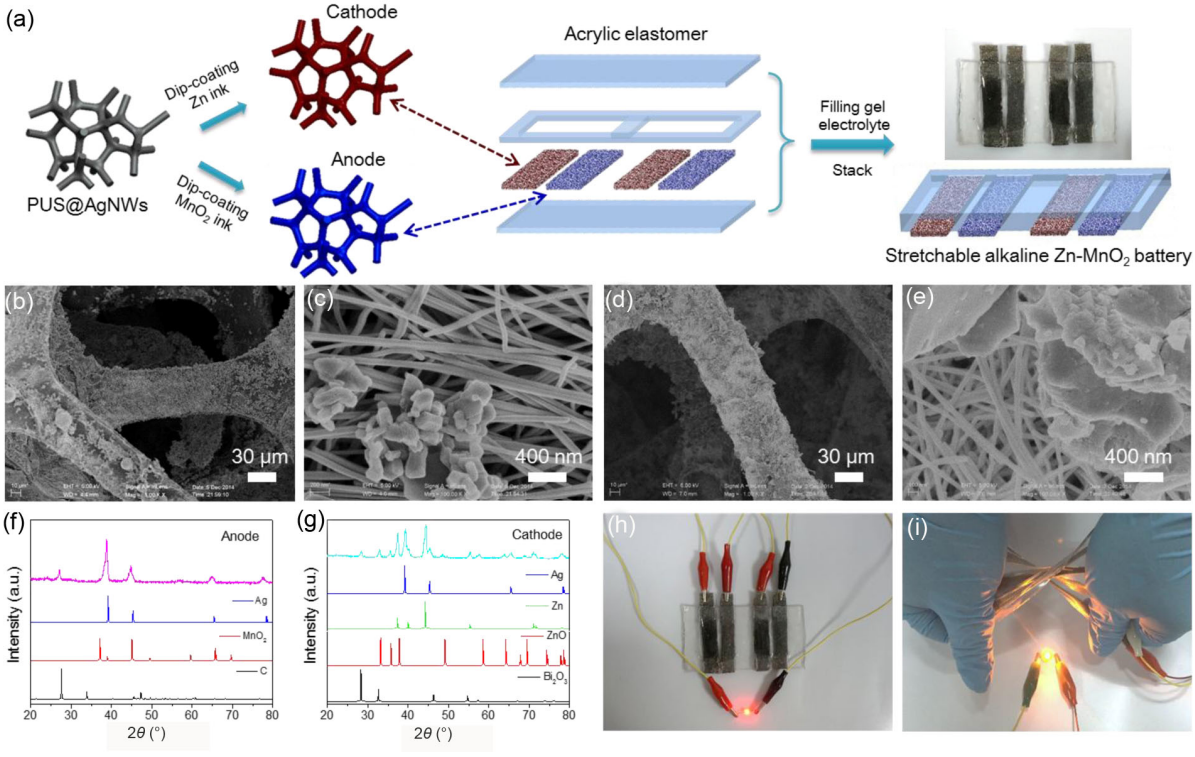

Figure 3 (a) Schematic illustration of the electrode and battery fabrication processes. SEM images of Zn particles ((b) and (c)) and MnO_2 particles ((d) and (e)) loaded on a PUS@AgNW current collector. (f) XRD patterns of the anode in (d) and (e) showing the presence of MnO_2, C, Ag, and PUS, and (g) the cathode in (b) and (c) showing the presence of Zn, Bi_2O_3, Ag, and PUS. (h) Optical images of as-fabricated stretchable full Zn-MnO_2 batteries connected in series. (i) The batteries connected in series powering a red LED under simultaneous stretching and twisting.

series [37]. As shown in Fig. 3(i), two connected Zn-MnO_2 stretchable batteries could light up a red LED (operating voltage 1.7–3.0 V with a 10 mA current; Fig. S5 in the ESM). The Zn-MnO_2 battery displayed high stretchability originating from the porous PUS@AgNW structure. The battery was still able to power a red LED even when it was simultaneously stretched to 100% strain in the x-direction and twisted by 90° in the z-direction (Fig. 3(i)).

The stretchable batteries provided a stable power supply under various levels of deformation. As shown in Fig. 4(a) and Video S1 in the ESM, the batteries lit up the red LED during stretching deformation up to 100% strain, indicating stable performance under uniaxial strain. On poking a marker pen into the sealed battery, which caused distortion, stretching, and pressuring all at the same time, the red LED remained lit up (Fig. S4 in the ESM). Discharge voltage curves for the batteries under 0, 50%, and 100% uniaxial stretch at a discharge current of 0.35 mA are shown in Fig. 4(b). These curves showed a minor voltage decrease in the ohmic loss ($I \times R$) and a small degradation in the battery upon stretching. The small capacity decrease (~ 1 mAh) during stretching deformation might arise from the electrical discontinuity due to the detachment of slurry particles from the AgNWs. The voltage curves for the battery under 100% strain at different discharge currents (0.35, 0.7, 1, and 2 mA) are shown in Fig. 4(c). The battery exhibited a capacity of 6.67 mAh, which decreased to 4.78 mAh at a current of 2 mA.

EIS measurements were performed to measure the inner resistance of the battery under different levels of strain [28]. The resistance determined from the high-frequency intercept with the x-axis was attributed to the electrolyte, electrode leads, and terminals. As shown in Fig. 4(d), the ohmic loss with the increasing strain indicated that the inner resistance of the battery increased with increasing deformation. However, even at 200% strain, the resistance was only 50 Ω. The

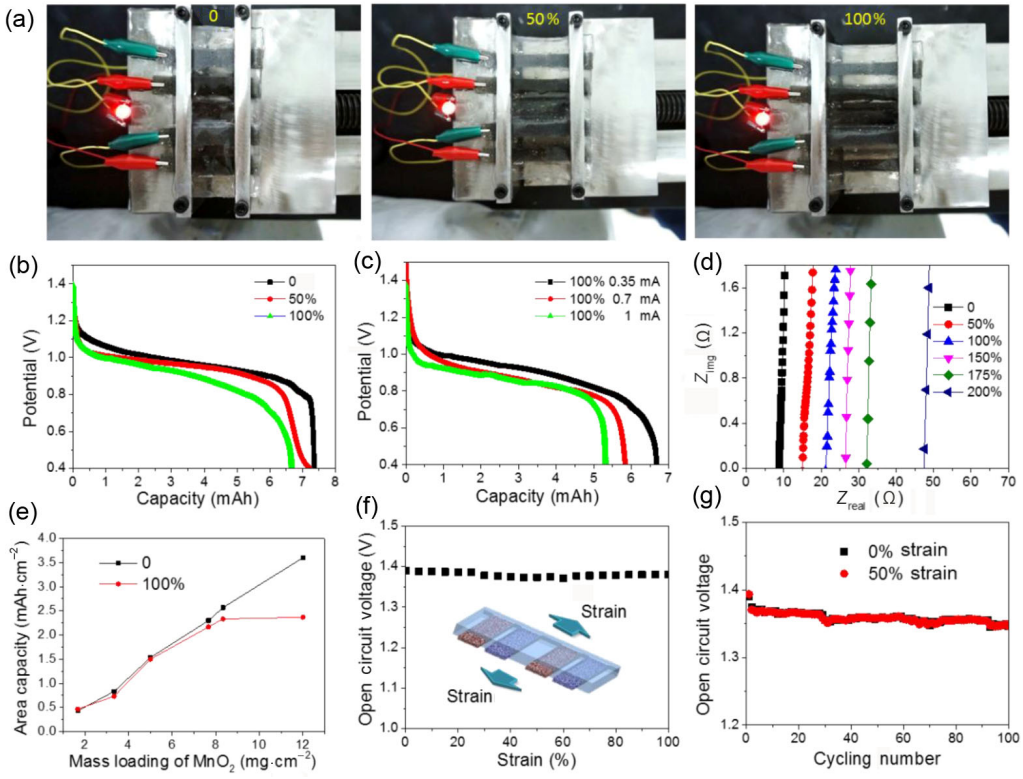

Figure 4 Stretchability of an alkaline Zn-MnO_2 full battery. (a) Optical images of two stretchable batteries connected in series powering a red LED under 0, 50%, and 100% strain. (b) Discharge curves for the battery at 0, 50%, and 100% strain at a discharge current of 0.35 mA. (c) Discharge curves for the battery under 100% strain at discharge currents of 0.35, 0.7, 1, and 2 mA. (d) EIS curves for the full battery at 0, 50%, 100%, 150%, 175%, and 200% strain. (e) Influence of MnO_2 mass loading on the area-capacity performance of the battery under 0 and 100% strain. (f) OCV of the battery during deformation up to 100% strain. (g) OCV of battery during 100 repeated deformations to 50% strain.

ionic conduction pathways under large strain beyond a recoverable level were still maintained, which might be a result of the positive effects of the viscous and cohesive ionic-gel electrolyte. The capacity of the battery could be further optimized by adjusting the mass loading of the active materials. Using a typical ink concentration (130 mg·mL^{-1}), the mass loading of MnO_2 (specific capacity of 308 mAh·g^{-1}) was ~ 45 mg·cm^{-2}. The mass loading of Zn (specific capacity: 825 mAh·g^{-1}) was ~ 90 mg·cm^{-2}, which provides almost 5 times the capacity of the cathode. Thus, the capacity of the battery was limited by the mass loading of MnO_2. Figure 4(e) shows that the battery capacity increased linearly with increasing the MnO_2 mass loading, while maintaining the Zn excess, up to 3.6 mAh·cm^{-2} at a mass loading of 12 mg·cm^{-2} and 0 deformation strain. The Zn-MnO_2 battery is a primary battery and, thus, could not be recharged. However, the areal capacity was quite competitive compared with recently reported stretchable primary batteries, and had an obvious advantage of secondary batteries (Table S1 in the ESM). Under 100% strain, the battery capacity did not increase with increasing mass loading beyond 7.7 mg·cm^{-2}. Thus, to ensure optimal battery performance under 100% strain, a mass loading of 7.7 mg·cm^{-2} was used, which provided a capacity of 2.3 mAh·cm^{-2}.

The battery stability under repeated stretching was also evaluated. Figure 4(f) shows a negligible drop in the battery OCV (from 1.4 to 1.39 V) as a function of the stretch strain (up to 100%). The OCV was also measured over 100 repeated stretches at 50% strain (Fig. 4(g)). The OCV (1.35 V) did not diminish over 100 stretches, indicating that the electrochemically active particles anchored on the PUS@AgNW current collector were quite stable. In other words, the battery possessed good mechanical-electric properties, and

could stably power an electric circuit during repeated stretching, thus meeting the requirements for component-level stretchability [7].

4 Conclusions

In summary, we have fabricated a highly stretchable Zn-MnO_2 battery via a facile dip-coating method, using a AgNW-coated sponge (PUS@AgNW) with a binary network as a stretchable current collector. The PUS@AgNW current collector consisted of stretchable commercial PUS and conductive AgNW networks, and possessed excellent conductivity (up to 50 $S \cdot cm^{-1}$) and stretchability (up to 100% strain). The Zn-MnO_2-battery cathode and anode were fabricated by dip-coating PUS@AgNW current collectors in electrochemically active particles. The 3D binary-network electrodes not only effectively minimized the strain, but also stably trapped the electrochemically active materials, during repeated stretching deformation. The capacity of the stretchable battery reached 3.6 $mAh \cdot cm^{-2}$. Under 100% strain, the battery still maintained 89% of its capacity, and could provide stable power at currents of 0.35, 0.7, and 1 mA. In contrast to traditional methods used to build up spatial structures, we fabricated a 3D porous electrode using off-the-shelf PUS. The dip-coating method is compatible with mainstream industrial processing and, thus, our stretchable-battery fabrication can easily be scaled up. Such a stretchable battery with high capacity is quite attractive for use as a power source in future wearable devices.

Acknowledgements

We acknowledge the funding support from the National Natural Science Foundation of China (Nos. 21431006 and 21761132008), the Foundation for Innovative Research Groups of the National Natural Science Foundation of China (No. 21521001), Key Research Program of Frontier Sciences, CAS (No. QYZDJ-SSW-SLH036), the National Basic Research Program of China (No. 2014CB931800), and the Users with Excellence and Scientific Research Grant of Hefei Science Center of CAS (No. 2015HSC-UE007).

Electronic Supplementary Material: Supplementary material (supplementary video, SEM images, optical images, EDS mapping, *I*–*V* curve, detailed methods and stretchablility characterizations of acrylic-AgNWs film) is available in the online version of this article at https://doi.org/10.1007/s12274-017-1771-4.

References

[1] Pan, S. W.; Yang, Z. B.; Chen, P. N.; Deng, J.; Li, H. P.; Peng, H. S. Wearable solar cells by stacking textile electrodes. *Angew. Chem., Int. Ed.* **2014**, *126*, 6224–6228.

[2] Song, Y. M.; Xie, Y. Z.; Malyarchuk, V.; Xiao, J. L.; Jung, I.; Choi, K.-J.; Liu, Z. J.; Park, H.; Lu, C. F.; Kim, R.-H. et al. Digital cameras with designs inspired by the arthropod eye. *Nature* **2013**, *497*, 95–99.

[3] Lipomi, D. J.; Vosgueritchian, M.; Tee, B. C. K.; Hellstrom, S. L.; Lee, J. A.; Fox, C. H.; Bao, Z. N. Skin-like pressure and strain sensors based on transparent elastic films of carbon nanotubes. *Nat. Nanotechnol.* **2011**, *6*, 788–792.

[4] Kim, D.-H.; Lu, N. S.; Ma, R.; Kim, Y.-S.; Kim, R.-H.; Wang, S. D.; Wu, J.; Won, S. M.; Tao, H.; Islam, A. et al. Epidermal electronics. *Science* **2011**, *333*, 838–843.

[5] Yamada, T.; Hayamizu, Y.; Yamamoto, Y.; Yomogida, Y.; Izadi-Najafabadi, A.; Futaba, D. N.; Hata, K. A stretchable carbon nanotube strain sensor for human-motion detection. *Nat. Nanotechnol.* **2011**, *6*, 296–301.

[6] Melzer, M.; Kaltenbrunner, M.; Makarov, D.; Karnaushenko, D.; Karnaushenko, D.; Sekitani, T.; Someya, T.; Schmidt, O. G. Imperceptible magnetoelectronics. *Nat. Commun.* **2015**, *6*, 6080.

[7] Yao, S. S.; Zhu, Y. Nanomaterial-enabled stretchable conductors: strategies, materials and devices. *Adv. Mater.* **2015**, *27*, 1480–1511.

[8] Bandodkar, A. J.; Nunez-Flores, R.; Jia, W.; Wang, J. All-printed stretchable electrochemical devices. *Adv. Mater.* **2015**, *27*, 3060–3065.

[9] Xie, K. Y.; Wei, B. Q. Materials and structures for stretchable energy storage and conversion devices. *Adv. Mater.* **2014**, *26*, 3592–3617.

[10] Yu, C. J.; Masarapu, C.; Rong, J. P.; Wei, B. Q.; Jiang, H. Q. Stretchable supercapacitors based on buckled single-walled carbon-nanotube macrofilms. *Adv. Mater.* **2009**, *21*, 4793–4797.

[11] Hyun, D. C.; Park, M.; Park, C.; Kim, B.; Xia, Y. N.; Hur, J. H.; Kim, J. M.; Park, J. J.; Jeong, U. Ordered zigzag stripes of polymer gel/metal nanoparticle composites for highly stretchable conductive electrodes. *Adv. Mater.* **2011**, *23*, 2946–2950.

[12] Gray, D. S.; Tien, J.; Chen, C. S. High-conductivity elastomeric electronics. *Adv. Mater.* **2004**, *16*, 393–397.

[13] Xu, S.; Zhang, Y. H.; Cho, J.; Lee, J.; Huang, X.; Jia, L.; Fan, J. A.; Su, Y. W.; Su, J.; Zhang, H. G. et al. Stretchable batteries with self-similar serpentine interconnects and integrated wireless recharging systems. *Nat. Commun.* **2013**, *4*, 1543.

[14] Song, Z. M.; Ma, T.; Tang, R.; Cheng, Q.; Wang, X.; Krishnaraju, D.; Panat, R.; Chan, C. K.; Yu, H. Y.; Jiang, H. Q. Origami lithium-ion batteries. *Nat. Commun.* **2014**, *5*, 3140.

[15] Kwon, Y. H.; Woo, S.-W.; Jung, H.-R.; Yu, H. K.; Kim, K.; Oh, B. H.; Ahn, S.; Lee, S.-Y.; Song, S.-W.; Cho, J. et al. Cable-type flexible lithium ion battery based on hollow multi-helix electrodes. *Adv. Mater.* **2012**, *24*, 5192–5197.

[16] Yan, C. Y.; Wang, X.; Cui, M. Q.; Wang, J. Q.; Kang, W. X.; Foo, C. Y.; Lee, P. S. Stretchable silver-zinc batteries based on embedded nanowire elastic conductors. *Adv. Energy. Mater.* **2014**, *4*, 1301396.

[17] Park, J.; Wang, S. D.; Li, M.; Ahn, C.; Hyun, J. K.; Kim, D. S.; Kim do, K.; Rogers, J. A.; Huang, Y. G.; Jeon, S. Three-dimensional nanonetworks for giant stretchability in dielectrics and conductors. *Nat. Commun.* **2012**, *3*, 916.

[18] Sekitani, T.; Noguchi, Y.; Hata, K.; Fukushima, T.; Aida, T.; Someya, T. A rubberlike stretchable active matrix using elastic conductors. *Science* **2008**, *321*, 1468–1472.

[19] Sun, Y. M.; Lopez, J.; Lee, H.-W.; Liu, N.; Zheng, G. Y.; Wu, C.-L.; Sun, J.; Liu, W.; Chung, J. W.; Bao, Z. et al. A stretchable graphitic carbon/Si anode enabled by conformal coating of a self-healing elastic polymer. *Adv. Mater.* **2016**, *28*, 2455–2461.

[20] Lee, S.; Shin, S.; Lee, S.; Seo, J.; Lee, J.; Son, S.; Cho, H. J.; Algadi, H.; Al-Sayari, S.; Kim, D. E. et al. Ag nanowire reinforced highly stretchable conductive fibers for wearable electronics. *Adv. Funct. Mater.* **2015**, *25*, 3114–3121.

[21] Kim, Y.; Zhu, J.; Yeom, B.; Di Prima, M.; Su, X. L.; Kim, J.-G.; Yoo, S. J.; Uher, C.; Kotov, N. A. Stretchable nanoparticle conductors with self-organized conductive pathways. *Nature* **2013**, *500*, 59–63.

[22] Chen, X. L.; Lin, H. J.; Deng, J.; Zhang, Y.; Sun, X. M.; Chen, P. N.; Fang, X.; Zhang, Z. T.; Guan, G. Z.; Peng, H. S. Electrochromic fiber-shaped supercapacitors. *Adv. Mater.* **2014**, *26*, 8126–8132.

[23] Yang, Z. B.; Deng, J.; Chen, X. L.; Ren, J.; Peng, H. S. A highly stretchable, fiber-shaped supercapacitor. *Angew. Chem., Int. Ed.* **2013**, *52*, 13453–13457.

[24] Ren, J.; Zhang, Y.; Bai, W. Y.; Chen, X. L.; Zhang, Z. T.; Fang, X.; Weng, W.; Wang, Y. G.; Peng, H. S. Elastic and wearable wire-shaped lithium-ion battery with high electrochemical performance. *Angew. Chem., Int. Ed.* **2014**, *126*, 7998–8003.

[25] Park, M.; Im, J.; Shin, M.; Min, Y.; Park, J.; Cho, H.; Park, S.; Shim, M. B.; Jeon, S.; Chung, D. Y. et al. Highly stretchable electric circuits from a composite material of silver nanoparticles and elastomeric fibres. *Nat. Nanotechnol.* **2012**, *7*, 803–809.

[26] Chun, K.-Y.; Oh, Y.; Rho, J.; Ahn, J.-H.; Kim, Y.-J.; Choi, H. R.; Baik, S. Highly conductive, printable and stretchable composite films of carbon nanotubes and silver. *Nat. Nanotechnol.* **2010**, *5*, 853–857.

[27] Lang, X. Y.; Hirata, A.; Fujita, T.; Chen, M. W. Nanoporous metal/oxide hybrid electrodes for electrochemical supercapacitors. *Nat. Nanotechnol.* **2011**, *6*, 232–236.

[28] Gaikwad, A. M.; Zamarayeva, A. M.; Rousseau, J.; Chu, H.; Derin, I.; Steingart, D. A. Highly stretchable alkaline batteries based on an embedded conductive fabric. *Adv. Mater.* **2012**, *24*, 5071–5076.

[29] Kettlgruber, G.; Kaltenbrunner, M.; Siket, C. M.; Moser, R.; Graz, I. M.; Schwödiauer, R.; Bauer, S. Intrinsically stretchable and rechargeable batteries for self-powered stretchable electronics. *J. Mater. Chem. A* **2013**, *1*, 5505–5508.

[30] Ge, J.; Yao, H.-B.; Wang, X.; Ye, Y.-D.; Wang, J.-L.; Wu, Z.-Y.; Liu, J.-W.; Fan, F.-J.; Gao, H.-L.; Zhang, C.-L. et al. Stretchable conductors based on silver nanowires: Improved performance through a binary network design. *Angew. Chem., Int. Ed.* **2013**, *52*, 1654–1659.

[31] Pan, H. L.; Shao, Y. Y.; Yan, P. F.; Cheng, Y. W.; Han, K. S.; Nie, Z. M.; Wang, C. M.; Yang, J. H.; Li, X. L.; Bhattacharya, P. et al. Reversible aqueous zinc/manganese oxide energy storage from conversion reactions. *Nat. Energy* **2016**, *1*, 16039.

[32] Lee, J.-Y.; Connor, S. T.; Cui, Y.; Peumans, P. Solution-processed metal nanowire mesh transparent electrodes. *Nano Lett.* **2008**, *8*, 689–692.

[33] Chen, M. T.; Zhang, L.; Duan, S. S.; Jing, S. L.; Jiang, H.; Li, C. Z. Highly stretchable conductors integrated with a conductive carbon nanotube/graphene network and 3D porous poly(dimethylsiloxane). *Adv. Funct. Mater.* **2014**, *24*, 7548–7556.

[34] Friis, E. A.; Lakes, R. S.; Park, J. B. Negative Poisson's ratio polymeric and metallic foams. *J. Mater. Sci.* **1988**, *23*, 4406–4414.

[35] Gaikwad, A. M.; Whiting, G. L.; Steingart, D. A.; Arias, A. C. Highly flexible, printed alkaline batteries based on mesh-embedded electrodes. *Adv. Mater.* **2011**, *23*, 3251–3255.

[36] Kaltenbrunner, M.; Kettlgruber, G.; Siket, C.; Schwödiauer, R.; Bauer, S. Arrays of ultracompliant electrochemical dry gel cells for stretchable electronics. *Adv. Mater.* **2010**, *22*, 2065–2067.

[37] Gaikwad, A. M.; Steingart, D. A.; Nga Ng, T.; Schwartz, D. E.; Whiting, G. L. A flexible high potential printed battery for powering printed electronics. *Appl. Phys. Lett.* **2013**, *102*, 233302.